RSC Advances

PAPER

View Article Online
View Journal | View Issue

Cite this: *RSC Adv.*, 2017, **7**, 53135

Removal of Cu(II) from aqueous solution using Fe_3O_4–alginate modified biochar microspheres

Changjiang Yu,[ab] Miao Wang,[b] Xinyu Dong,[b] Zaifeng Shi,[b] Xiaopeng Zhang[b] and Qiang Lin *[ab]

Magnetic microspheres (MM) were prepared using calcium alginate (CA) encapsulated biochar (BC) and Fe_3O_4 as a high-performance green absorbent for Cu(II) removal from aqueous solution. The effects of the initial Cu(II) concentration, initial pH value of the Cu(II) solution and equilibrium contact time were investigated. The results revealed that the adsorption capacity of MM was approximately 3 times higher than that of the magnetic biochar (MBC). The adsorption of Cu(II) by the MM was in good agreement with pseudo-second-order kinetics. The overall orders for fitting the isotherm models are Langmuir > Freundlich for Cu(II). Mechanism studies showed that coordination and ion exchange were the major mechanism for Cu(II) removal by the MM. Moreover, the presence of the magnetic particles in the microspheres allowed easy separation of the material from aqueous solutions. This study provides an effective method for biochar modification.

Received 13th September 2017
Accepted 13th November 2017

DOI: 10.1039/c7ra10185f

rsc.li/rsc-advances

1. Introduction

Copper is an essential micro-nutrient needed by human beings, animals and plants at low levels, while it is toxic beyond certain limits and can also cause serious environmental issues.[1] Copper can be accumulated by living organisms throughout the food chain as a highly toxic and non-biodegradable pollutant, causing adverse effects on humans.[2] Adsorption is an effective technology for pollutant removal. However, most commercial adsorbents have limited capability for heavy metal removal while the cost remains as another issue. Biochar is usually generated from incomplete pyrolysis of carbon-rich materials and is considered cost-effective and favorable for heavy metals removal.[3]

Despite the attractiveness of biochar, one limitation for the wide application is that biochar is difficult to recycle from the treated wastewater. To tackle this, magnetic separation is a promising approach for easy and efficient recovery of solid materials. As a result, magnetically modified biochar has been widely investigated in removal of dyes and heavy metals from aqueous solution.[4–6] Chemical co-precipitation of magnetic components and biochar is an easy method to prepare magnetic composite materials.[7,8] The magnetic modification can improve the adsorption capacity of the hybrid biochar,[7–10] while some reports have found that the efficiency of adsorption by magnetically modified biochar was correlated to its structure.[11,12] In this regard, the magnetic modification has a negative impact on the adsorption capacity of biochar with poorly developed structure.[11–13]

Particularly, magnetic particles on the surface of biochar may impair the adsorption of heavy metals by functional groups (*e.g.* carboxylic and hydroxyl). Moreover, the surface loaded magnetic particles, as one can imagine, can be decomposed in acidic solutions.

Sodium alginate is a natural polymer, extracted from marine brown algae. It has great biocompatibility and biodegradability and possesses majorly β-1,4-glycosidic linked α-L-mannuronic acid and β-D-guluronic acid.[14] Sodium alginate could form three-dimensional gel by the exchange of sodium ions from the β-D-guluronic acid with the divalent cations (*e.g.* Ca^{2+}), which is widely used as encapsulating compounds and composite materials.[15,16] The resulting CA has been widely used to immobilize small particles material, such as nanoporous MCM-41,[17] graphene oxide,[18] halloysite nanotube,[18] activated carbon,[19] silica[20] and magnetic nanoparticles,[21] in order to adsorb heavy metals and dyes from aqueous solutions.

This study aims at providing a better way which can address the drawback of magnetic biochar. A magnetic microsphere (MM) was prepared using CA encapsulated biochar and Fe_3O_4 for Cu(II) removal from aqueous solution. A series of adsorption experiments were conducted to compare the adsorption ability of MM and the biochars with and without magnetic modification for Cu(II). The adsorption characteristics of Cu(II) and the effects of experimental conditions have been systemically investigated. The mechanism of Cu(II) adsorption on CA/BC–Fe_3O_4 magnetic microsphere is discussed based on characterization of the materials.

[a]*Faculty of Environmental Science and Engineering, Kunming University of Science and Technology, No. 68 Wenchang Road, Kunming 650093, China. E-mail: linqianggroup@163.com*

[b]*Key Laboratory of Water Pollution Treatment & Resource Reuse of Hainan Province, College of Chemistry and Chemical Engineering, Hainan Normal University, No. 99 Longkunnan Road, Haikou 571158, China*

2. Materials and methods

2.1 Materials

Sodium alginate was purchased from Shanghai jingchun Technology Co. Ltd. (Shanghai, China), $FeCl_3 \cdot 6H_2O$, $FeSO_4 \cdot 7H_2O$, $CaCl_2$ and NaOH were purchased from Guangzhou chemical reagent factory (Guangzhou, China), $Cu(NO_3)_2 \cdot 3H_2O$ and $NaNO_3$ were purchased Aladdin Holdings Group, Cu standard liquid was purchased Shanghai fusheng Co. Ltd. (Shanghai, China). All chemicals with analytical grade were used without further purification.

2.2 Preparation of biochar

Coconut shell was collected from a suburb (Haikou, China), air-dried at 70 °C and ground to pass a 0.074 mm sieve. The obtained powders were used as the feedstock and pyrolyzed under nitrogen conditions in a tube furnace to produce biochar (BC). The pyrolysis temperature was raised to 200 °C at 5 °C min^{-1} with a further step heating up to 700 °C at 10 °C min^{-1} and held for 3 hours.[22] The biochars were naturally cooled to room temperature and stored in airtight plastic bags.

2.3 Preparation of magnetic biochar

The magnetic biochar (MBC) was synthesized according to a modified co-precipitation method.[4,9,10] $FeCl_3 \cdot 6H_2O$ (0.006 M) and $FeSO_4 \cdot 7H_2O$ (0.003 M) were added to distilled water (150 mL) under nitrogen atmosphere. Biochars (2 g) were added to above mixture and stirred for 30 min. Under vigorous mechanical stirring, NaOH solution (5 M) was added dropwise to adjust the pH to 11. The stirring continued for 1 hour and the suspension was aged at room temperature for 10 hours. The filtrate was separated by a magnet and washed with distilled water, and ethanol (3 times). The obtained magnetic biochars were dried at 50 °C in an air oven.

2.4 Preparation of magnetic particles

Fe_3O_4 particles were prepared through a modified hydrothermal method.[23] $FeCl_3 \cdot 6H_2O$ (0.08 M) was dissolved in 300 mL ultra-pure water and stirred for 0.5 hour. $FeSO_4 \cdot 7H_2O$ (0.04 M) was dissolved separately in 100 mL ultra-pure water and then slowly added to $FeCl_3$ solution with constant stirring under the protection of nitrogen atmosphere. Thereafter, NaOH (10 M) was added dropwise to above mixture to increase the pH to 11 and stirred for 30 min at 75 °C. The mixture was transferred to a kettle and continued to react at 160 °C for 5 hours to obtain magnetic particles. Finally, the magnetic particles were separated with a magnet and washed with water, ethanol and acetone, and dried in a vacuum oven at 70 °C for 8 hours.

2.5 Preparation of CA/BC–Fe_3O_4 magnetic microsphere (MM)

The CA/BC–Fe_3O_4 magnetic microspheres were prepared according to a modified method.[24–27] 3 g of sodium alginate was dissolved into 150 mL of ultra-pure water. Then 3 g of Fe_3O_4 was added to sodium alginate solution and vigorously stirred for 2 hours. 6 g of biochars were added into 150 mL of deionized water and stirred for 2 hours. The biochars suspension was slowly dropped into the viscous solution of sodium alginate and stirred continuously to form a homogeneous mixed solution. The obtained suspension was then dropped carefully into $CaCl_2$ solution (0.2 M) to form CA/BC–Fe_3O_4 magnetic microsphere. The microspheres were kept in $CaCl_2$ solution for 6 hours. The obtained magnetic microsphere were then washed with ultra-pure water (eight times) and separated with a magnet, dried at 60 °C in an air oven. CA microspheres were obtained by dropping a solution composed of 1% (w/v) of sodium alginate into $CaCl_2$ solution (0.2 M). The post-processing methods of CA were the same as those of MM.

2.6 Characterization

The Cu(II) concentration was analyzed using an atomic absorption spectrophotometer (AAS, AA-7000, Shimadzu, Japan). The morphology of samples was investigated with a scanning electron microscopy equipped with (SEM, JSM-7401F, JEOL, Japan). In addition, surface element analysis was also conducted simultaneously with SEM, using energy dispersive X-ray spectroscopy (EDS). Structural and compositional characteristics of the materials were investigated by X-ray diffraction (UItima IV, Rigaku, Japan). X-ray photoelectron spectroscopy(XPS, PHI5000 Versaprobe-II, Ulvac-Phi, Japan) was used to analyze the chemical composition of the magnetic microspheres. The magnetic property was determined using a magnetic property measurement system (7404, LakeShore, USA). The Fourier transform infrared (FTIR) spectra were measured by using Nicolet 6700 infrared spectroscope (Thermo Electro Corp, USA). The thermal stability was analyzed using a TG-DSC instrument (STA 449 F3, Netzsch, USA).

2.7 Adsorption kinetic study

The adsorption experiments of BC, MBC, CA, and MM were carried out at room temperature (25 ± 1 °C). A stock solution of 80 mg L^{-1} Cu(II) was prepared by dissolving $Cu(NO_3)_2$ in a 0.01 mol L^{-1} $NaNO_3$ solution as a back-ground electrolyte at pH 5.[22] pH value of the solutions was adjusted using either 0.1 M HNO_3 or 0.1 M NaOH solutions. 0.1 g of the biochars or magnetic biochars was introduced into 50 mL of Cu(II) solution in conical flasks. The flasks were placed into an incubator shaker and shaken at a constant speed (160 rpm) for a certain period of time (10 min to 32 h). After shaking, the biochars and the magnetic biochars were filtered and the concentrations of Cu(II) in the filtered solutions were analyzed using a flame atomic absorption spectrometer.[28] A certain amount of the MM or CA were introduced into 500 mL of Cu(II) solution in a beaker under magnetic stirring. 1 mL of Cu(II) solution was withdrawn at different times and tested after dilution.[29] All the results were obtained by taking an average of three specimens. The kinetic experiment methods for all types of adsorbents are reasonable,[30–32] which can accurately reflect their adsorption kinetic characteristics. The adsorption capacity of Cu(II) at time t (q_t) was then calculated using eqn (1).

$$q_t = \frac{(C_0 - C_t)V}{m} \quad (1)$$

where C_0 (mg L^{-1}) is the initial Cu(II) ion concentration; C_t (mg L^{-1}) is the Cu(II) ion concentration at time t; V is the volume (L) of Cu(II) ion solution and m is the dry weight (g) of the adsorbent used.

2.8 Adsorption isotherm study

The BC, MBC, CA, and MM were respectively introduced into different concentrations (40–300 mg L^{-1}) of Cu(II) solution at room temperature (25 ± 1 °C) in a 0.01 mol L^{-1} $NaNO_3$ solution as a back-ground electrolyte and shaken at a constant speed (160 rpm) for 24 h.[33] The quantification method of Cu(II) is the same as the kinetic study. All the results were obtained by taking an average of three specimens. The equilibrium adsorption capacity of Cu(II) (q_e) was calculated using eqn (2).

$$q_e = \frac{(C_0 - C_e)V}{m} \quad (2)$$

where C_0 (mg L^{-1}) and C_e are the initial and equilibrium concentrations of Cu(II) ions, respectively; V is the volume (L) of Cu(II) solution and m is the dry weight (g) of adsorbent used.

2.9 Desorption experiment

The reusability of MM was evaluated using consecutive adsorption–desorption cycles.[34] The adsorption experiments were repeated by using the same MM. 0.1 g of metal-loaded MM was shaken in the desorbing agent (HNO_3 100 mL of 0.1 mol L^{-1}) in a 250 mL Erlenmeyer at 160 rpm in a shaker for 120 min at room temperature.[16] The concentration of Cu(II) in the acidic solution was measured using AAS. All the results were obtained by taking an average of three specimens.

3. Results and discussion

3.1 Characterization of materials

3.1.1 SEM analysis. The biochar (BC) showed a clear porous structure while magnetic biochar (MBC) was covered by ferro-ferric oxide on the surface (Fig. 1A and B). In the latter case the original porous structure of BC was shielded.

The SEM images of the surface and section of MM are shown in Fig. 1C and D. Biochar and Fe_3O_4 were at intervals imbedded in three-dimensional network of MM. The surface area of MM is 12.18 m^2 g^{-1}, which is microporous.

3.1.2 XRD analysis. X-ray diffraction (XRD) is an effective method to confirm the existence of Fe_3O_4 in composites. Fig. 2 shows the XRD patterns of prepared Fe_3O_4 nanoparticles (a), magnetic biochar (b) and MM (c). The diffraction peaks at 2θ = 30.1°, 35.5°, 43.1°, 53.5°, 57.0°, 62.6°, and 74.0° are assigned to the (2 2 0), (3 1 1), (4 0 0), (4 2 2), (5 1 1), (4 4 0), and (5 3 3) planes, respectively, which agree well with the database of Fe_3O_4 standard card (JCPDS no. 65-3107).[35] No impurity peak is observed in the XRD pattern, which indicates that the Fe_3O_4 particles are highly crystalline cubic spinel structure.[36,37]

3.1.3 Magnetic properties. The hysteresis loops of Fe_3O_4 nanoparticle (a) and magnetic microsphere (b) are shown in Fig. 3. There were no remanence or coercivity, which indicated that the adsorbents exhibited typical superparamagnetic behavior.[38,39] The result showed that the maximum saturation magnetization of Fe_3O_4 and MM were 60.8 emu g^{-1}, 11.75 emu g^{-1} respectively. Thus, the MM can be separated readily between the liquid and solid phase by using a magnet.[34]

3.1.4 Thermal analysis. Thermogravimetric analysis was used to assess the thermal stability of CA and MM. CA had three stages of mass loss as shown in Fig. 4. The initial mass loss, from room temperature to 180 °C, was attributed to the release of crystal water and the moisture evaporation.[30] The second step for degradation of CA appeared around 180–440 °C, which might be associated with the fracture of glycosidic bonds, decarboxylation, decarbonylation and dehydration of alginate.[40] The third step was situated at 440–710 °C, resulting from the further thermal degradation of formed residues.[29,41] The MM also had three stages of mass loss and the TG curve trend was

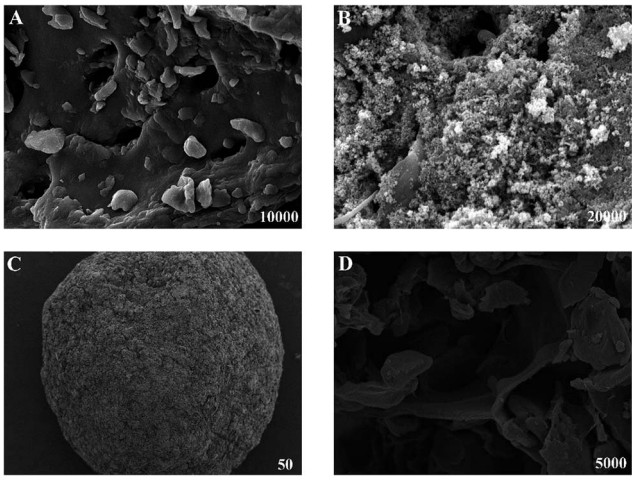

Fig. 1 SEM images of (A) BC, (B) MBC, (C) the outside surface of MM, (D) the section of MM.

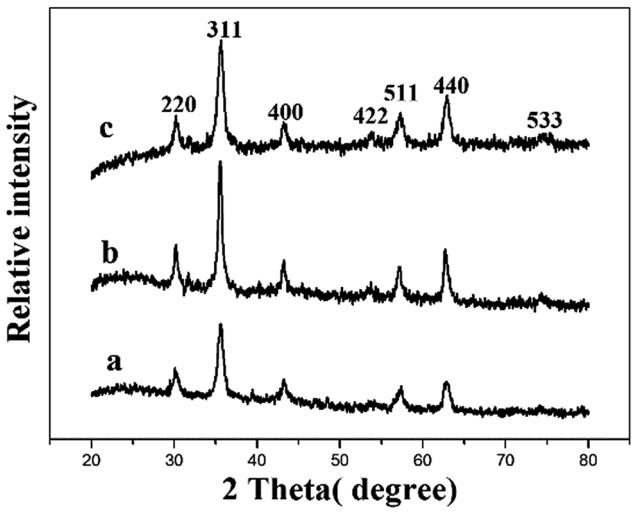

Fig. 2 XRD pattern of Fe_3O_4 nanoparticle (a), magnetic biochar (b) and magnetic microsphere (c).

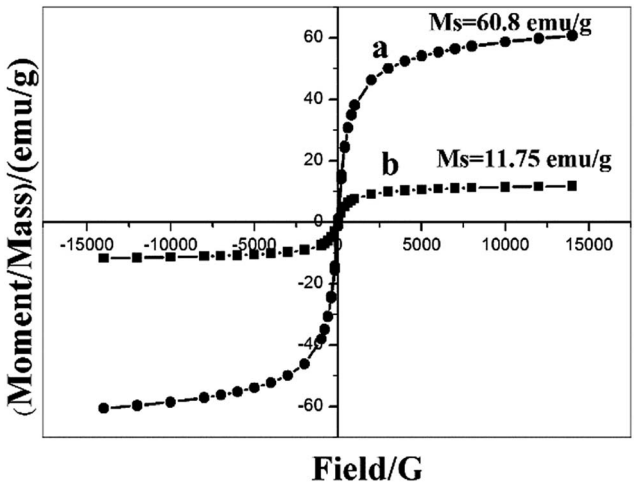

Fig. 3 The magnetization curve of Fe_3O_4 nanoparticle (a) and magnetic microsphere (b).

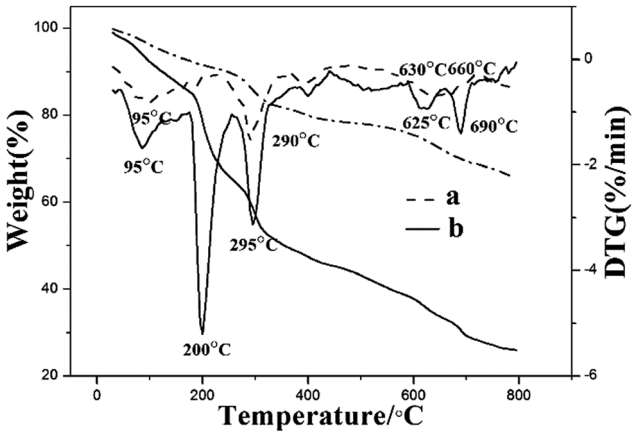

Fig. 4 TG curves of magnetic microsphere (a) and calcium alginate (b).

similar to CA. The main difference is that the second step of degradation for MM appeared around 230 °C, which is higher than CA about 180 °C. This result was likely attributed to the additional energy required for bond cleavage after the addition of biochar and Fe_3O_4. The reason might be hydrogen bonds were formed between the hydroxyl group and the carbonyl group or Fe–O group.[42] The results of TG showed that the thermostability of MM was more stable than that of CA.

3.2 Effect of pH on adsorption and stability

The effect of pH on the adsorption capacity of MM was investigated. The adsorption experiments were carried out at an initial Cu(II) concentration of 60 mg L^{-1} in 0.01 mol L^{-1} $NaNO_3$ solution as a back-ground electrolyte. This study was carried out in a pH range from 2 to 6 since Cu(II) ions may start to precipitate above pH 6.[3] All the results were obtained by taking an average of three specimens. When pH increased, the sorption capacity of Cu(II) increased quickly (Fig. 5A). This can be explained by the fact that at the lower pH, more protons (H^+) were characterized by high mobility and competed with the metal ions for the active sites on the adsorbents. When increasing the pH, the concentration of H^+ ions decreased, resulting in more Cu(II) absorbed.[43] The pH value of the solution increased significantly after the adsorption of Cu(II). The main reason could be that the alkali metal oxide on biochar dissolved in acid solution.[28] In order to enhance the accuracy of the experiment, pH = 5 was chosen as the optimum experiment condition.[44] After the adsorption, Fe_3O_4 decomposition rate was calculated using eqn (3).

$$S = \frac{C_e V M_{Fe_3O_4}}{3 M_{Fe} m} \quad (3)$$

where S is Fe_3O_4 decomposition rate, C_e (mg L^{-1}) is the final concentrations of Fe ions, M_{Fe} and $M_{Fe_3O_4}$ are the molecular weight of Fe and Fe_3O_4, V is the volume (L) of solution, and m is the weight (mg) of Fe_3O_4 in adsorbents used. The Fe_3O_4 content of CA/BC–Fe_3O_4 (1 : 2 : 1) magnetic microsphere is about 25% of the microsphere. The Fe_3O_4 decomposition rate of magnetic biochars was analyzed using the same methods. The magnetic biochars was disposed by nitric acid and the total content of Fe_3O_4 was measured. Fig. 5B showed that the Fe_3O_4 decomposition rate of MM was significantly less than those of MBC with pH lower than 3. Therefore, MM has high chemical stability than MBC in acidic solution.

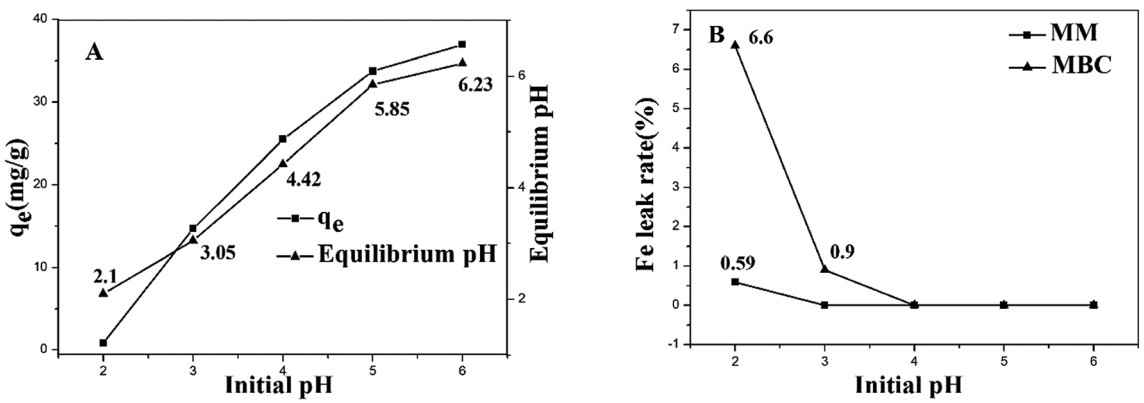

Fig. 5 Effect of pH on the adsorption of Cu(II) by MM (A) and Fe decomposition rate in the solution (B).

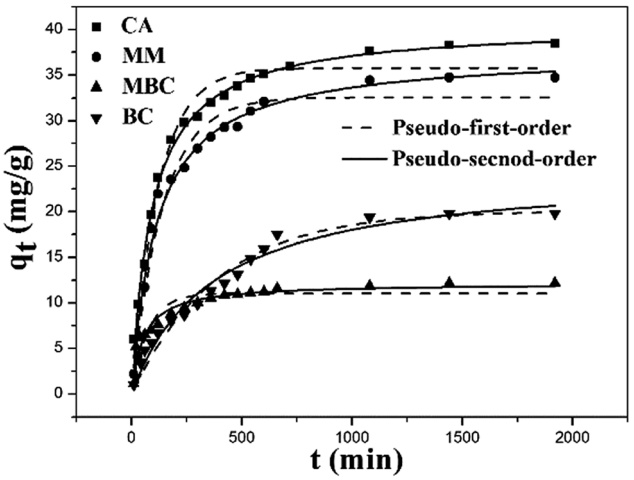

Fig. 6 Kinetic adsorption plots of Cu(II) by CA, MM, MBC and BC.

Table 1 Kinetics parameter coefficients for Cu(II) adsorption onto BC, MBC, MM and CA

	Pseudo-first-order model			Pseudo-second-order model		
Sample	$q_{e,cal}$	k_1 (10^{-3})	R^2	$q_{e,cal}$	k_2 (10^{-4})	R^2
BC	20.08	2.57	0.9724	24.63	1.1	0.9770
MBC	11.07	13.23	0.8691	12.17	15.5	0.9497
MM	32.57	7.09	0.9644	37.49	2.34	0.9811
CA	35.77	8.32	0.9677	40.51	2.68	0.9934

3.3 Kinetics adsorption experiments

The kinetic behavior of the Cu(II) ion removal by different adsorbents used in this work was investigated by using the dynamic data. Pseudo-first-order kinetic model and pseudo-second-order kinetic model were applied to deal with the data, which are described in eqn (4) and (5).[17,45] The results for non-linear curve fitting to the dynamic data were shown in Fig. 6.

$$\log(q_e - q_t) = \log q_e - \left(\frac{k_1}{2.303}\right)t \quad (4)$$

$$\frac{t}{q_t} = \frac{1}{k_2 q_e^2} + \frac{t}{q_e} \quad (5)$$

where, q_t and q_e are the amounts of Cu(II) ions removed per unit mass of adsorbent in mg g^{-1} at an arbitrary contact time t (s) and at equilibrium stage. k_1, k_2 is the pseudo-first-order kinetic constant and pseudo-second-order kinetic constant expressed in min^{-1}, g mg^{-1} min^{-1}, respectively.

The kinetic model parameters as well as correlation coefficient (R^2) for each adsorbent are included in Table 1.

It can be seen that the correlation coefficients (R^2) for BC was nearly comparable to pseudo-first-order equation (0.9724) and pseudo-second-order equation (0.9770) model. The adsorption capacity obtained from pseudo-second-order equation fitting values was consistent with the experimental result, which suggested that the rate limiting step was governed by diffusion while the chemical adsorption also played a crucial role.[46] The main reason is due to the porous nature of biochar.

The pseudo-second-order equation did describe the adsorption results of Cu(II) onto MBC. The correlation coefficients (0.9497) for MBC was superior compared to pseudo-first-order equation (0.8691) indicating that the chemisorption is the rate-controlling step.[31] The main reason is that the surface of biochar was covered by ferroferric oxide, which shielded the porous structure of biochar.

The correlation coefficients of the pseudo-second-order kinetic model for MM and CA were 0.9811 and 0.9934. They are higher than the correlation coefficient derived from the pseudo-first-order model for MM (0.9644) and CA (0.9677). In addition, the adsorption capacity obtained from pseudo-second-order equation fitting values was consistent with the experiment result. All these results highlighted the chemisorption rate-controlling mechanism.[47]

The data showed that the kinetic constant of MBC was the highest. This could be the fact that the absorption was mainly happening on the surface of MBC. The kinetic constant of MM is higher than that of BC, indicating that MM has improved the adsorption rate of biochar. The adsorption kinetic constants of MM, CA and BC are relatively lower than MBC. The reason could be that the Cu(II) ion was gradually diffused to the interior of MM, CA and BC. This process needed more time.

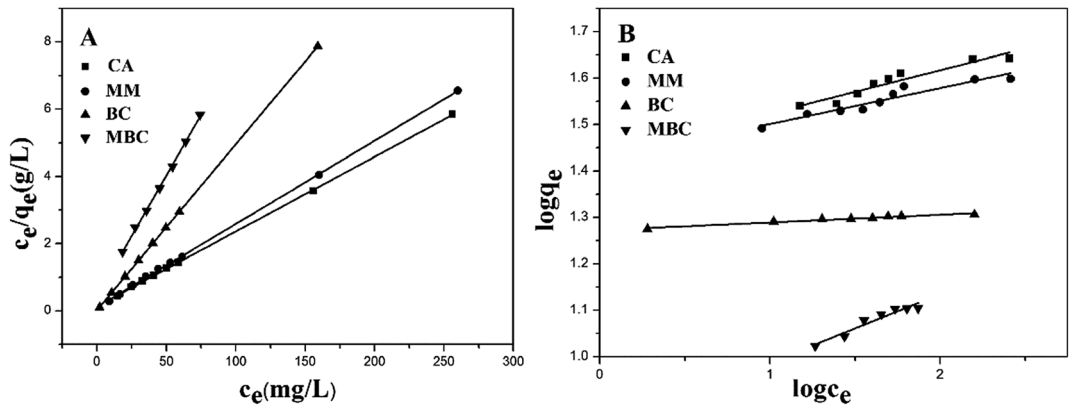

Fig. 7 Adsorption isotherms of Langmuir (A) and Freundlich (B) equations for the adsorption of Cu(II) ion by CA, MM, BC and MBC.

Table 2 Isotherm parameters of Cu(II) sorption onto BC, MBC, MM and CA

	Langmuir			Freundlich		
Sample	q_m	K_L	R^2	$1/n$	K_F	R^2
BC	20.28	2.0342	0.9999	0.0162	18.7283	0.9608
MBC	13.87	0.1680	0.9987	0.1477	6.9087	0.9226
MM	40.42	0.2168	0.9996	0.0775	26.5216	0.9097
CA	44.98	0.1602	0.9998	0.0730	26.9649	0.9086

Table 3 Physical properties of the MM and CA

Material	BET Surface Area ($m^2\ g^{-1}$) ($m^2\ g^{-1}$)	Pore volume ($cm^3\ g^{-1}$)	Average pore diameter (nm)
MM	12.18	0.036	10.06
CA	2.72	0.009	3.14

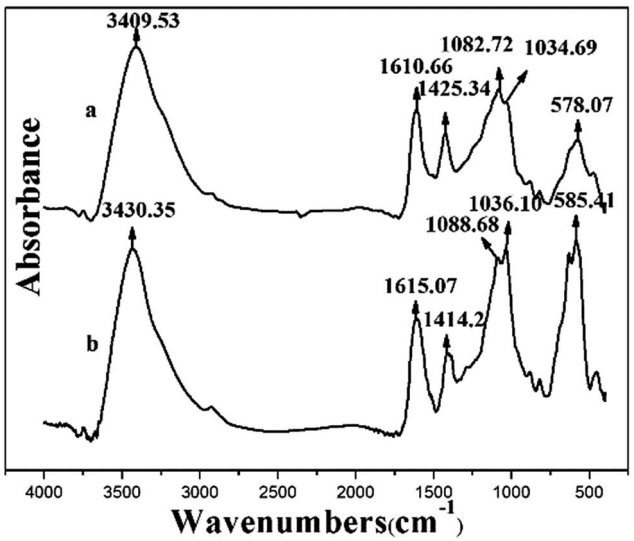

Fig. 8 FTIR of MM before (a) and after (b) Cu(II) adsorption.

3.4 Isotherms adsorption experiments

The adsorption isotherms were studied using the Langmuir and Freundlich isotherm models. The Langmuir isotherm model is described as eqn (6).[18]

$$\frac{C_e}{q_e} = \frac{1}{K_L q_m} + \frac{C_e}{q_m} \quad (6)$$

where, C_e (mg L^{-1}) is the concentration of Cu(II) ions at equilibrium. q_m (mg g^{-1}) is the Langmuir adsorption maximum. K_L is the coefficient of distribution of the adsorption. q_e is the amount of Cu(II) ions removed per unit mass of adsorbent in mg g^{-1} at equilibrium stage.

The Freundlich isotherms model is described as eqn (7).[48]

$$\log q_e = \log K_F + \frac{1}{n} \log C_e \quad (7)$$

K_F is the coefficient of distribution of the adsorption.

The Langmuir and Freundlich isotherms for all types of adsorbents are shown in Fig. 7. The results showed that the Cu(II) ion adsorption increases rapidly when a low initial Cu(II) ion concentration was used and then gradually reaches a maximum with increased Cu(II) ion concentration.

The isotherms model parameters as well as the correlation coefficient (R^2) for each adsorbent are reported in Table 2.

As shown in Table 2, the correlation coefficients R^2 of the Langmuir model adsorption isotherm plots are high, 0.9999, 0.9987, 0.9996 and 0.9998 for the BC, MBC, MM and CA, respectively. The R^2 suggest that the Langmuir model fits the adsorption data well. The reason may be due to the homogeneous nature of active sites on the adsorbents, a monolayer adsorption occurred between the adsorbents and Cu(II) ions.[20,49] The q_m value of the MBC is determined to be 13.87 mg g^{-1}, which is lower than that of biochar. Again, the surface of MBC covered with ferroferric oxide could impair the adsorption of heavy metals by functional groups in the biochar.

Table 3 shows the specific surface area, pore volume and average pore diameter of MM and CA.

It turned out that the BET surface area, pore volume and average pore diameter of MM are higher than that of CA, which is expected to be advantageous for metal ions diffusion (*e.g.* Cu^{2+} in this study). In addition, the combination of MM largely increases the colloidal stability of biochar and thus avoids the agglomeration problem.

When biochars and Fe_3O_4 were encapsulated in CA, the q_m increased to 40.42 mg g^{-1}. It is closer to the value of CA in the previous literature (at 42.7 mg g^{-1}) and those in this study (at

Table 4 Comparison of various adsorbents for copper removal from water

Adsorbents	pH	Concentration range (mg L^{-1})	Q_{max} (mg g^{-1})	Ref.
Amino modification biochar	5	10–300	16.13	51
$KMnO_4$ modified biochar	5	2–250	12.3	52
Chitosan magnetic nanoparticles	5	10–2000	21.5	53
Multi-walled carbon nanotubes	5	10–30	12.34	54
Chitosan-montmorillonite composite	5	2–100	34.9	55
Graphene oxide aerogel	6	50–75	19.65	56
Sodium alginate magnetic nanocomposite	7	50	18.11	57
Surfactant-modified hydroxyapatite/zeolite composite	6	10–60	38.1	58
Alginate/biochar magnetic microspheres	5	40–300	40.42	This study

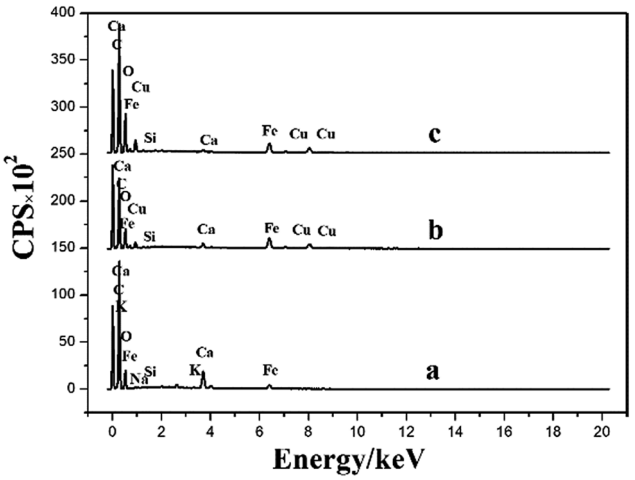

Fig. 9 SEM-EDS patterns of MM before Cu(II) adsorption (a), the surface (b) and section (c) of MM after Cu(II) adsorption.

44.98 mg g^{-1}).[30] Due to the content of CA in CA/BC–Fe_3O_4 (1 : 2 : 1) magnetic microsphere is only 25%, it appears a synergistic effect between biochar and Fe_3O_4 in CA, which enhances the maximum adsorption capacity of Cu(II) ion.

The estimated adsorption cost required by the biochars is about 19% as much as that by the CA.[50] Therefore, the obtained MM is a low-cost and high efficiency adsorbent for Cu(II) removal from aqueous solution.

3.5 Comparison with other adsorbents

The adsorption capacity (q_m value) for Cu(II) on MM is comparable with reported adsorbents as shown in Table 4. It can be seen that MM is suitable and promising for the removal of Cu(II) from aqueous solutions since it has a relatively high adsorption capacity.

3.6 Adsorption mechanism

3.6.1 FTIR analysis. FTIR is used to determine the molecular interactions and analyze functional groups of MM before and after Cu(II) adsorption. In Fig. 8, for the magnetic microsphere a stretching vibration peak of O–H at 3409.53 cm^{-1}, an asymmetric stretching peak of COO^- at 1610.66 cm^{-1},[15] a bending vibration peak of CH_2 at 1425.34 cm^{-1},[30] and a stretching vibration peak of Fe–O at 578.07 cm^{-1} were observed.[59] The peaks between 1082.72 cm^{-1} and 1034.69 cm^{-1} are the stretching vibrations of C–O–C and Si–O.[28,60] The FTIR spectra of MM after Cu(II) adsorption showed that some adsorption peaks generated slight displacements. The O–H, COO^-, Fe–O, C–O–C and Si–O wavelengths after Cu(II) adsorption were longer to a certain extent than those before Cu(II) adsorption.[61] This result may be attributed to functional groups coordinated to Cu(II).[62]

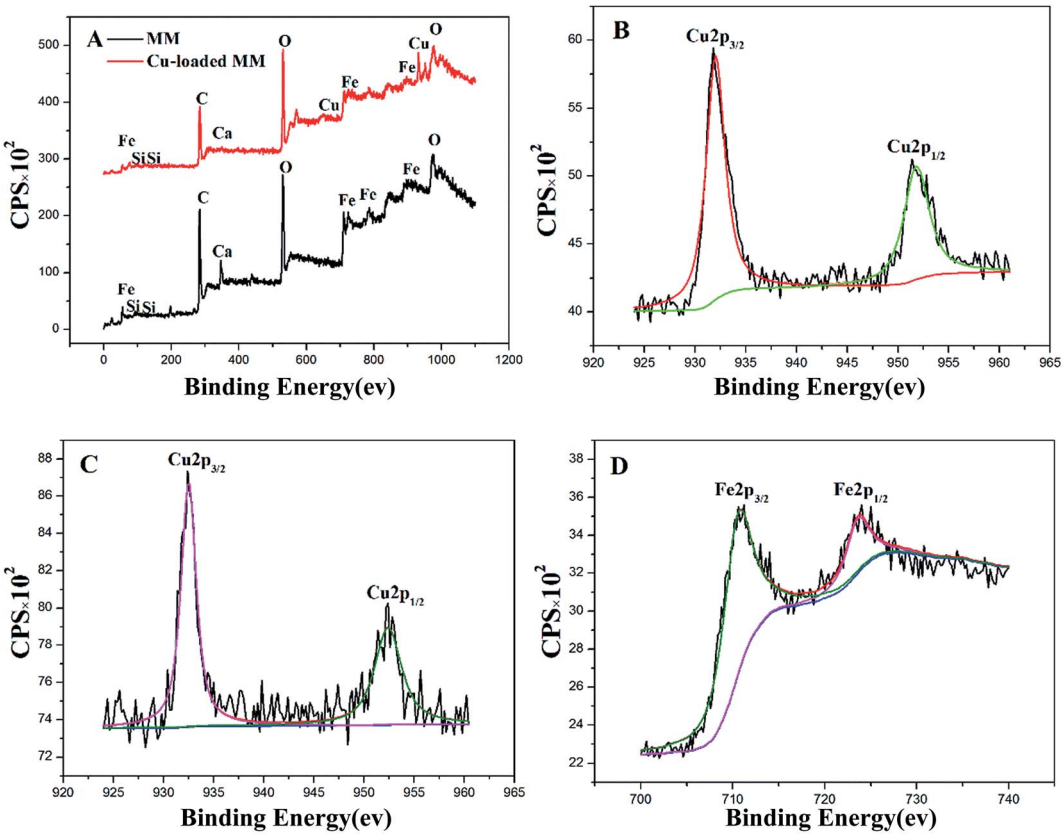

Fig. 10 XPS wide scan spectra of MM and Cu-loaded MM (A), Cu 2p for MM after Cu(II) adsorption (B), Cu 2p for MBC after Cu(II) adsorption (C), Fe 2p for MM after Cu(II) adsorption (D).

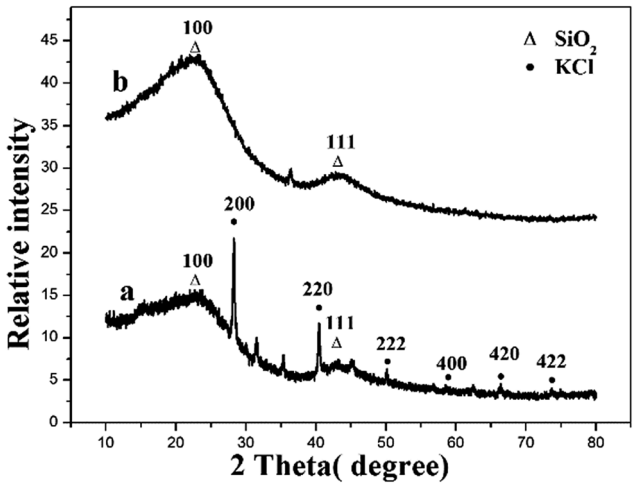

Fig. 11 XRD pattern of biochar before (a) and after (b) Cu(II) adsorption.

3.6.2 SEM-EDS analysis. SEM-EDS patterns of MM before Cu(II) adsorption (a), the surface (b) and section (c) of MM after Cu(II) adsorption are shown in Fig. 9. The SEM-EDX studies revealed that the weight% of Ca(II) (8.77 to 2.40, 0.78) ions in MM decreased after loading Cu(II) onto MM. Due to the MM was uneven, the metal content in different parts of MM varied slightly. However, it is still clear that the weight% of Ca(II) decreased significantly, which indicated Cu(II) exchanging Ca(II) happened on the MM.[63] The weight% of Cu(II) on the surface and section of MM are 10.65% and 14.54% respectively, which show that Cu(II) ions are relatively homogenously adsorbed on the surface and internal of MM.

3.6.3 XPS analysis. Fig. 10A showed the typical XPS wide scan spectra of MM before and after Cu(II) adsorption. A new peak appeared after Cu(II) adsorption, which is in agreement with Cu(II) standard data.[62] In addition, Ca(II) ions in MM were reduced obviously after Cu(II) adsorption, which is in accordance with the result of SEM-EDS. Fig. 10B and C showed the Cu 2p spectrum of Cu(II)-loaded MM and MBC. The peaks at 932, 932.5 eV and 951.8, 952.4 eV could be ascribed to Cu $2p_{3/2}$ and Cu $2p_{1/2}$, respectively. The binding energies of Cu $2p_{3/2}$ and Cu $2p_{1/2}$ were centered at 934.1 and 952.55 eV, respectively.[64,65] A significant shift for Cu 2p to low binding energies was observed after Cu(II) adsorption onto MM and MBC, suggesting that coordination or ion exchange reaction occurred between Cu(II) and MM or MBC. Fig. 10D showed the Fe 2p spectrum of Cu(II)-loaded MM. The peaks at 710.5 and 723.58 eV could be ascribed to Fe $2p_{3/2}$ and Fe $2p_{1/2}$, respectively. The binding energies of Fe $2p_{3/2}$ and Fe $2p_{1/2}$ for Fe_3O_4 were centered at 711.1 and 724.8 eV, respectively.[66] A significant shift for Fe 2p to low binding energies was also observed after Cu(II) adsorption onto MM, suggesting that coordination reaction occurred between Cu(II) and Fe_3O_4.

3.6.4 XRD analysis. XRD pattern of biochar before (a) and after (b) Cu(II) adsorption are shown in Fig. 11. The diffraction peaks at $2\theta = 28.3°$, 40.5°, 50.1°, 58.6°, 66.3° and 73.7° are assigned to the (2 0 0), (2 2 0), (2 2 2), (4 0 0), (4 2 0) and (4 2 2) planes, respectively, which agree well with the database of KCl standard card (JCPDS no. 41-1476).[67] The diffraction peaks at $2\theta = 22.0°$ and 42.0° are assigned to the (2 0 0) and (4 2 2) planes, respectively. The angular position of the diffraction line corresponded to the amorphous structure SiO_2, in accordance with the data contained in the database JCPDS-ICDD.[68] The XRD pattern of loaded Cu(II) on biochars did not show new peaks, indicating that the precipitation reactions did not occur on the surface of the biochars. The mechanisms responsible for Cu(II) ion sorption by biochars are surface interactions (*e.g.* ion exchange, coordination) and formation of precipitates with inorganic components.[1,3] Therefore, copper removal by biochar should be controlled by surface interactions. Fig. 11 showed some peaks of the biochar disappeared after absorption. This result may be attributed to some inorganic salts (*e.g.* KCl) dissolved in water in the process of adsorption.

3.7 Proposed mechanism

The difference of magnetic microsphere before and after Cu(II) loading has been distinguished by FTIR, SEM-EDS and XPS. The sorption mechanism is proposed in Fig. 12. The functional groups (Fe–O, O–H, Si–O and COO^-) played a key role in the removal. The nature of Cu(II) abstraction took place through the ion exchange between Ca(II) and Cu(II) as well as the formation of coordination complex.

3.8 Recyclability

The used magnetic alginate microspheres were recycled and used as regenerated absorbent for four repeated sorption–

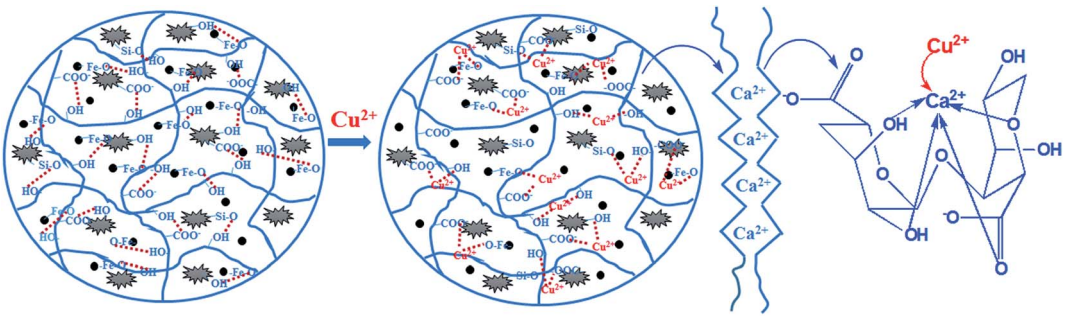

Fig. 12 The mechanism of Cu(II) adsorption.

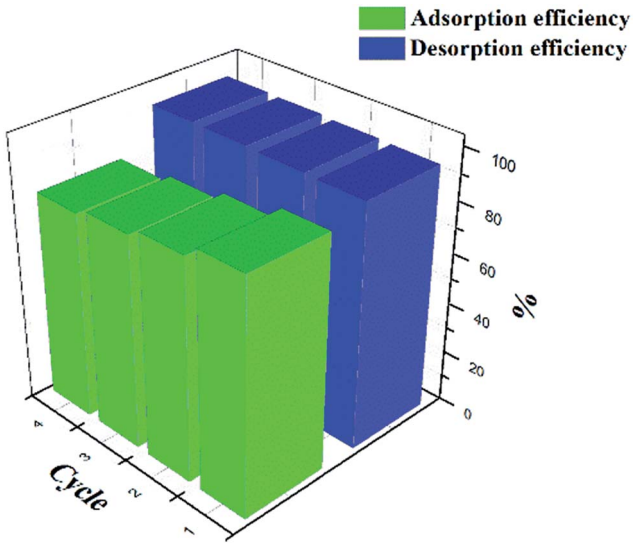

Fig. 13 Recycle tests for Cu(II) adsorption onto MM.

desorption cycles (Fig. 13). The efficiency of Cu(II) was approximate 96%, which is stable and sufficiently high. The adsorption capacity of Cu(II) decreased by 9.2% in the second cycle. In the subsequent cycles, the adsorption capacity decreased slowly, therefore, the total loss of adsorption capacity throughout the 4 cycles was 19.4%. Fe_3O_4 decomposition rate was 1.5% in the first desorption, in addition, the total loss of Fe_3O_4 throughout the 4 cycles was 3.1%. There is no significant damage was observed and the spherical shape of magnetic alginate microspheres was well maintained.

4. Conclusions

In summary, we have shown that the MM has high chemical stability and adsorption capacity than MBC. It appears a synergistic effect between biochar and Fe_3O_4 in CA, which enhances the maximum adsorption capacity of Cu(II) ion. The maximum adsorption capacity of the MM from the Langmuir equation was 40.42 mg g^{-1}. The magnetic microsphere showed 80.6% of the initial Cu(II) adsorption capacity after 4 cycles reuse. This research provides an effective way for biochar modification and may have great value for the application of biochar in water treatment.

Conflicts of interest

There are no conflicts to declare.

Acknowledgements

This work was supported by the Key Research and Development Project of Hainan Province of China (Project No. ZDYF2017102), Natural Science Foundation of Hainan Province of China (Project No. 20162032) and Hainan Provincial Fine Chemical Engineering Research Center opening topic fund subsidization.

References

1 X.-j. Tong, J.-y. Li, J.-h. Yuan and R.-k. Xu, *Chem. Eng. J.*, 2011, **172**, 828–834.
2 F. M. Pellera, A. Giannis, D. Kalderis, K. Anastasiadou, R. Stegmann, J. Y. Wang and E. Gidarakos, *J. Environ. Manage.*, 2012, **96**, 35–42.
3 M. Li, Q. Liu, L. Guo, Y. Zhang, Z. Lou, Y. Wang and G. Qian, *Bioresour. Technol.*, 2013, **141**, 83–88.
4 M. Y. Khan, A. S. Mangrich, J. Schultz, F. S. Grasel, N. Mattoso and D. H. Mosca, *J. Anal. Appl. Pyrolysis*, 2015, **116**, 42–48.
5 S. Y. Wang, Y. K. Tang, K. Li, Y. Y. Mo, H. F. Li and Z. Q. Gu, *Bioresour. Technol.*, 2014, **174**, 67–73.
6 S. Y. Wang, Y. K. Tang, C. Chen, J. T. Wu, Z. Huang, Y. Y. Mo, K. X. Zhang and J. B. Chen, *Bioresour. Technol.*, 2015, **186**, 360–364.
7 X. F. Tan, Y. G. Liu, Y. L. Gu, Y. Xu, G. M. Zeng, X. J. Hu, S. B. Liu, X. Wang, S. M. Liu and J. Li, *Bioresour. Technol.*, 2016, **212**, 318–333.
8 K. R. Thines, E. C. Abdullah, N. M. Mubarak and M. Ruthiraan, *Renewable Sustainable Energy Rev.*, 2017, **67**, 257–276.
9 D. Mohan, H. Kumar, A. Sarswat, M. Alexandre-Franco and C. U. Pittman, *Chem. Eng. J.*, 2014, **236**, 513–528.
10 B. Chen, Z. Chen and S. Lv, *Bioresour. Technol.*, 2011, **102**, 716–723.
11 Z. Han, B. Sani, W. Mrozik, M. Obst, B. Beckingham, H. K. Karapanagioti and D. Werner, *Water Res.*, 2015, **70**, 394–403.
12 L. Trakal, V. Veselska, I. Safarik, M. Vitkova, S. Cihalova and M. Komarek, *Bioresour. Technol.*, 2016, **203**, 318–324.
13 D. Mohan, P. Singh, A. Sarswat, P. H. Steele and C. U. Pittman Jr, *J. Colloid Interface Sci.*, 2015, **448**, 238–250.
14 R. D. C. Soltani, G. S. Khorramabadi, A. R. Khataee and S. Jorfi, *J. Taiwan Inst. Chem. Eng.*, 2014, **45**, 973–980.
15 A. F. Hassan, A. M. Abdel-Mohsen and H. Elhadidy, *Int. J. Biol. Macromol.*, 2014, **68**, 125–130.
16 X. Li, Y. Qi, Y. Li, Y. Zhang, X. He and Y. Wang, *Bioresour. Technol.*, 2013, **142**, 611–619.
17 H. Tavakoli, H. Sepehrian and R. Cheraghali, *J. Taiwan Inst. Chem. Eng.*, 2013, **44**, 343–348.
18 Y. Li, Q. Du, T. Liu, J. Sun, Y. Wang, S. Wu, Z. Wang, Y. Xia and L. Xia, *Carbohydr. Polym.*, 2013, **95**, 501–507.
19 A. Sigdel, W. Jung, B. Min, M. Lee, U. Choi, T. Timmes, S.-J. Kim, C.-U. Kang, R. Kumar and B.-H. Jeon, *Catena*, 2017, **148**, 101–107.
20 S. Zhang, F. Xu, Y. Wang, W. Zhang, X. Peng and F. Pepe, *Chem. Eng. J.*, 2013, **234**, 33–42.
21 A. Idris, N. S. M. Ismail, N. Hassan, E. Misran and A.-F. Ngomsik, *J. Ind. Eng. Chem.*, 2012, **18**, 1582–1589.
22 Y. Yang, Z. Wei, X. Zhang, X. Chen, D. Yue, Q. Yin, L. Xiao and L. Yang, *Bioresour. Technol.*, 2014, **171**, 227–232.
23 M. F. A. Taleb, *Carbohydr. Polym.*, 2014, **114**, 65–72.
24 K. W. Jung, T. U. Jeong, H. J. Kang and K. H. Ahn, *Bioresour. Technol.*, 2016, **211**, 108–116.

25 X. Cui, X. Dai, K. Y. Khan, T. Li, X. Yang and Z. He, *Bioresour. Technol.*, 2016, **218**, 1123–1132.
26 S. T. Danalıoğlu, Ş. S. Bayazit, Ö. Kerkez Kuyumcu and M. A. Salam, *J. Mol. Liq.*, 2017, **240**, 589–596.
27 S. Cataldo, A. Gianguzza, D. Milea, N. Muratore and A. Pettignano, *Int. J. Biol. Macromol.*, 2016, **92**, 769–778.
28 B. Zhou, Z. Wang, D. Shen, F. Shen, C. Wu and R. Xiao, *Ecol. Eng.*, 2017, **98**, 189–195.
29 T. Wu, L. Mao and H. Wang, *J. Fluorine Chem.*, 2017, **200**, 8–17.
30 W. M. Algothmi, N. M. Bandaru, Y. Yu, J. G. Shapter and A. V. Ellis, *J. Colloid Interface Sci.*, 2013, **397**, 32–38.
31 M. Zhang, B. Gao, S. Varnoosfaderani, A. Hebard, Y. Yao and M. Inyang, *Bioresour. Technol.*, 2013, **130**, 457–462.
32 C. Zhang, B. Shan, W. Tang and Y. Zhu, *Bioresour. Technol.*, 2017, **238**, 352–360.
33 Y. Guo, W. Tang, J. Wu, Z. Huang and J. Dai, *J. Environ. Sci.*, 2014, **26**, 2123–2130.
34 R. Verma, A. Asthana, A. K. Singh, S. Prasad and M. A. B. H. Susan, *Microchem. J.*, 2017, **130**, 168–178.
35 L. Yan, S. Li, H. Yu, R. Shan, B. Du and T. Liu, *Powder Technol.*, 2016, **301**, 632–640.
36 Y. Xu, Y. Zhou and R. Li, *Colloids Surf., A*, 2014, **459**, 240–246.
37 L. G. Yan, K. Yang, R. R. Shan, T. Yan, J. Wei, S. J. Yu, H. Q. Yu and B. Du, *J. Colloid Interface Sci.*, 2015, **448**, 508–516.
38 Y. Chen and S. Mu, *Sens. Actuators, B*, 2014, **192**, 275–282.
39 C. Yu, J. Geng, Y. Zhuang, J. Zhao, L. Chu, X. Luo, Y. Zhao and Y. Guo, *Carbohydr. Polym.*, 2016, **152**, 327–336.
40 C.-J. Zhang, Y. Liu, L. Cui, C. Yan and P. Zhu, *J. Anal. Appl. Pyrolysis*, 2016, **122**, 13–23.
41 N. E. Mousa, C. M. Simonescu, R.-E. Pătescu, C. Onose, C. Tardei, D. C. Culiță, O. Oprea, D. Patroi and V. Lavric, *React. Funct. Polym.*, 2016, **109**, 137–150.
42 E. Platero, M. E. Fernandez, P. R. Bonelli and A. L. Cukierman, *J. Colloid Interface Sci.*, 2017, **491**, 1–12.
43 N. Jiang, Y. Xu, Y. Dai, W. Luo and L. Dai, *J. Hazard. Mater.*, 2012, **215–216**, 17–24.
44 P. Regmi, J. L. Garcia Moscoso, S. Kumar, X. Cao, J. Mao and G. Schafran, *J. Environ. Manage.*, 2012, **109**, 61–69.
45 X. H. Do and B. K. Lee, *J. Environ. Manage.*, 2013, **131**, 375–382.
46 H. Jin, S. Capareda, Z. Chang, J. Gao, Y. Xu and J. Zhang, *Bioresour. Technol.*, 2014, **169**, 622–629.
47 W. Wang, L. Zong and A. Wang, *Int. J. Biol. Macromol.*, 2013, **62**, 225–231.
48 L. Liu, Y. Wan, Y. Xie, R. Zhai, B. Zhang and J. Liu, *Chem. Eng. J.*, 2012, **187**, 210–216.
49 B. Wang, C. Li and H. Liang, *Bioresour. Technol.*, 2013, **146**, 803–806.
50 X.-H. Do and B.-K. Lee, *J. Environ. Manage.*, 2013, **131**, 375–382.
51 G. X. Yang and H. Jiang, *Water Res.*, 2014, **48**, 396–405.
52 H. Wang, B. Gao, S. Wang, J. Fang, Y. Xue and K. Yang, *Bioresour. Technol.*, 2015, **197**, 356–362.
53 Y. C. Chang and D. H. Chen, *J. Colloid Interface Sci.*, 2005, **283**, 446–451.
54 I. Mobasherpour, E. Salahi and M. Ebrahimi, *J. Saudi Chem. Soc.*, 2014, **18**, 792–801.
55 C. Hu, G. Li, Y. Wang, F. Li, G. Guo and H. Hu, *Int. J. Biol. Macromol.*, 2017, **103**, 751–757.
56 X. Mi, G. Huang, W. Xie, W. Wang, Y. Liu and J. Gao, *Carbon*, 2012, **50**, 4856–4864.
57 M. M. Lakouraj, F. Mojerlou and E. N. Zare, *Carbohydr. Polym.*, 2014, **106**, 34–41.
58 Y. Zhan, J. Lin and J. Li, *Environ. Sci. Pollut. Res.*, 2013, **20**, 2512–2526.
59 A. R. Bagheri, M. Ghaedi, A. Asfaram, A. A. Bazrafshan and R. Jannesar, *Ultrason. Sonochem.*, 2017, **34**, 294–304.
60 B. Zhou, Z. Wang, D. Shen, F. Shen, C. Wu and R. Xiao, *Ecol. Eng.*, 2017, **98**, 189–195.
61 H. Ren, Z. Gao, D. Wu, J. Jiang, Y. Sun and C. Luo, *Carbohydr. Polym.*, 2016, **137**, 402–409.
62 Y. T. Zhou, C. Branford-White, H. L. Nie and L. M. Zhu, *Colloids Surf., B*, 2009, **74**, 244–252.
63 H. Roh, M.-R. Yu, K. Yakkala, J. R. Koduru, J.-K. Yang and Y.-Y. Chang, *J. Ind. Eng. Chem.*, 2015, **26**, 226–233.
64 H. Qiu, S. Zhang, B. Pan, W. Zhang and L. Lv, *J. Colloid Interface Sci.*, 2012, **366**, 37–43.
65 J. M. Lázaro Martínez, E. Rodríguez-Castellón, R. M. T. Sánchez, L. R. Denaday, G. Y. Buldain and V. Campo Dall' Orto, *J. Mol. Catal. A: Chem.*, 2011, **339**, 43–51.
66 H. Yuan, Y. Wang, S.-M. Zhou and S. Lou, *Chem. Eng. J.*, 2011, **175**, 555–560.
67 Y. Wang, H. Wu, Z. Sárossy, C. Dong and P. Glarborg, *Fuel*, 2017, **197**, 422–432.
68 T. Tański, W. Matysiak, Ł. Krzemiński, P. Jarka and K. Gołombek, *Appl. Surf. Sci.*, 2017, **424**, 184–189.

